

Conductance spectroscopy of topological superconductor wire junctions

F. Setiawan,¹ P. M. R. Brydon,¹ Jay D. Sau,¹ and S. Das Sarma¹

¹*Condensed Matter Theory Center and Joint Quantum Institute, Department of Physics,
University of Maryland, College Park, Maryland 20742-4111, USA*

(Dated: November 19, 2021)

We study the zero-temperature transport properties of one-dimensional normal metal-superconductor (NS) junctions with topological superconductors across their topological transitions. Working within the Blonder-Tinkham-Klapwijk (BTK) formalism generalized for topological NS junctions, we analytically calculate the differential conductance for tunneling into two models of a topological superconductor: a spinless intrinsic p -wave superconductor and a spin-orbit-coupled s -wave superconductor in a Zeeman field. In both cases we verify that the zero-bias conductance is robustly quantized at $2e^2/h$ in the topological regime, while it takes nonuniversal values in the nontopological phase. The conductance spectra in the topological state develops a peak at zero bias for certain parameter regimes, with the peak width controlled by the strength of spin-orbit coupling and barrier transparency.

PACS numbers: 74.45.+c, 73.40.-c, 03.67.Lx

I. INTRODUCTION

The search for topological superconductors in solid-state systems is motivated by the possibility of realizing Majorana zero-energy modes at their surfaces, which are of both fundamental and technological importance¹⁻³. In the absence of intrinsic topological superconductors, much effort has been put into engineering such systems from conventional components⁴⁻⁸. In addition to the proposals involving semiconductor-superconductor hybrid structures⁴⁻⁸ as hosts for Majorana modes, which have attracted considerable experimental attention⁹⁻¹⁵, there have been many recent theoretical proposals for artificially engineering effectively spinless low-dimensional p -wave topological superconductors¹⁶⁻²⁹, which could localize zero-energy Majorana modes at suitable defects such as vortex cores or system boundaries. The subject has been extensively reviewed in the recent literature³⁰⁻³³.

It is particularly desirable to realize spinless p -wave superconductors, as they support a single Majorana mode at their boundaries^{1,2}. The most promising of these proposals involves proximity-inducing superconductivity in a spin-orbit-coupled semiconducting nanowire in the presence of a magnetic field⁶⁻⁸, which has subsequently been the subject of a number of experiments⁹⁻¹⁵. By varying the magnetic field, the system is predicted to undergo a transition from a nontopological to a topological phase. Such an external magnetic-field-induced topological quantum phase transition has the considerable advantage of tuning the existence (or absence) of the Majorana mode in the experimental system simply by changing the Zeeman field. A key signature of the topologically nontrivial state is the quantized value $2e^2/h$ of the differential conductance for tunneling into the wire at zero-bias voltage. This quantized conductance, associated with perfect Andreev reflection, indicates the presence of a single localized Majorana zero-energy mode at the wire end³⁴⁻³⁸. For a sufficiently high tunnel barrier, the con-

ductance spectra will be peaked with this value at zero bias. While experimental results clearly show the development of such a peak upon tuning the system, at a finite magnetic field, into the predicted topological regime, the value of the zero-bias conductance peak is much less than the expected quantized value. The reasons for this discrepancy are addressed in Refs.^{39,40}, and alternative nontopological explanations have been advanced⁴¹⁻⁴⁶. The lack of quantization of the experimental observations can be reconciled^{5,39} with the Majorana theory by including the finite temperature and the finite length of the nanowire (thus allowing the Majorana modes from the two ends to overlap), but this physics is beyond the scope of our work where we restrict to zero temperature and a single normal metal-superconductor (NS) junction (assuming the other Majorana mode to be far away from this junction).

The difficulty in interpreting the tunneling experiments has prompted numerous theoretical studies on the conductance of the nanowire device, using both numerical^{39,45-52} and analytical techniques⁵³⁻⁵⁸. Although the latter works consider highly idealized models of the system, they are nevertheless valuable as they give clear insight into the parametric dependence of the transport physics as well as its dependence on various physical properties of the experimental setup, which can then be applied to understand the more complicated numerical studies. An important question concerns the change in the conductance as the system is tuned from the topologically trivial to the nontrivial regimes (e.g., by tuning the applied magnetic field in semiconductor-superconductor hybrid structures). Remarkably, this aspect of the physics has attracted relatively little attention using these analytic methods⁵⁵. The purpose of this paper is to analytically address this aspect of Majorana physics in topological nanowire junctions.

In this paper we examine the conductance spectra of one-dimensional NS junctions involving topological superconductors across their topological transition. We uti-

lize the Blonder-Tinkham-Klapwijk (BTK) formalism⁵⁹, which is commonly employed to study junctions with unconventional superconductors^{60–63}, to obtain analytic results for the tunneling conductance of two models of a topological superconductor junction: a junction between a spinless normal metal and a p -wave superconductor, and a junction between a spinful normal metal and a spin-orbit-coupled s -wave superconductor in a magnetic field. The former is the simplest model for tunneling into a topological superconductor^{54,56,57}, while the latter is a minimum model⁵ for the semiconductor nanowire device where experimental signatures for Majorana zero modes have been reported through the observation of zero-bias tunneling conductance peaks at the NS junction. We note that the spinless p -wave superconductor can be regarded as an effective low-energy theory for the semiconductor nanowire, but this is inadequate for understanding the conductance spectroscopy of the device. Our analysis is analytical, and in particular we give explicit expressions for the zero-bias tunneling conductance at zero temperature, which clearly shows an abrupt change at the topological transition. Specifically, we find that in the topological regime, the zero-temperature zero-bias conductance is quantized at a value of $2e^2/h$ independent of the barrier strength Z , but the detailed structure (e.g., the width and the shape) of the quantized zero-bias conductance peak is controlled by the barrier transparency and the magnitude of spin-orbit coupling. Our BTK theory for the topological NS junction also shows that a finite barrier transparency could lead to the experimentally observed soft gap which is ubiquitous in semiconductor nanowire tunneling experiments^{9,12–14}.

The paper is organized as follows. In Sec. II, we warm up by studying the conductance of a junction between a spinless normal metal and a spinless p -wave superconductor across the topological transition. We then generalize the theory to consider the semiconductor nanowire device in Sec. III. In particular, we obtain analytic results for the conductance spectra in the limits of a strong Zeeman field and strong spin-orbit coupling. Finally, the results are summarized in Sec. IV with a conclusion.

II. JUNCTION WITH A SPINLESS p -WAVE SUPERCONDUCTOR

We start by considering a one-dimensional junction between a spinless normal metal (NM) and a p -wave superconductor (p SC), which are located at $x \leq 0$ and $x \geq 0$, respectively. Their interface at $x = 0$ is modeled by a δ -function barrier of strength Z following the BTK prescription. The parameter Z controls the barrier transparency at the NS interface, and is the key parameter in the theory quantifying the tunneling conductance properties at the junction: a low (high) value of Z corresponds to a barrier with high (low) transparency at the NS interface. A microscopic evaluation of Z is typically difficult since the microscopic details of

the junction are generally unknown, and so Z is treated as a free fitting parameter. The Hamiltonian in each region is written $H_j(x) = \frac{1}{2} \int dx \Psi_j^\dagger(x) \mathcal{H}_j(x) \Psi_j(x)$, where $\Psi_j(x) = (\psi_j^\dagger(x), \psi_j(x))^T$ are Nambu spinors and $\psi_j^\dagger(x)$ ($\psi_j(x)$) denotes the creation (annihilation) field operator in region $j = N$ (NM) and p (p SC). Assuming that the mass m is uniform throughout the system, the Bogoliubov-de Gennes (BdG) Hamiltonians are

$$\mathcal{H}_N(x) = (-\hbar^2 \partial_x^2 / 2m - \mu_N) \tau_z, \quad (1a)$$

$$\mathcal{H}_p(x) = (-\hbar^2 \partial_x^2 / 2m - \mu_p) \tau_z - i \Delta_p \partial_x \tau_x, \quad (1b)$$

where μ_N (μ_p) is the chemical potential of the NM (p SC), $\Delta_p \geq 0$ is the p -wave pairing potential, and τ_μ are the Pauli matrices acting on the particle-hole space.

For notational simplicity, in the following we work with units such that \hbar , μ_N , and $2m$ are all equal to unity. The energy spectra of the NM and p SC are then given by $\epsilon_{N,\pm}(k) = \pm(k^2 - 1)$ and $\epsilon_{p,\pm}(k) = \pm \sqrt{(k^2 - \mu_p)^2 + (\Delta_p k)^2}$, respectively. In Fig. 1 we plot the spectrum of the p SC for different values of μ_p . Note that the spectrum becomes gapless at $\mu_p = 0$ which marks the topological transition¹ between the BEC-like strong pairing phase ($\mu_p < 0$) and the BCS-like weak pairing phase ($\mu_p > 0$). In the latter case, the positive energy spectrum only develops the characteristic “double-well” BCS structure for $\mu_p > \Delta_p^2/2$, with minimum value $E_1 = \Delta_p \sqrt{\mu_p - \Delta_p^2/4}$ at $k = \pm \sqrt{\mu_p - \Delta_p^2/2}$, and a local maximum value $E_2 = \mu_p$ at $k = 0$.

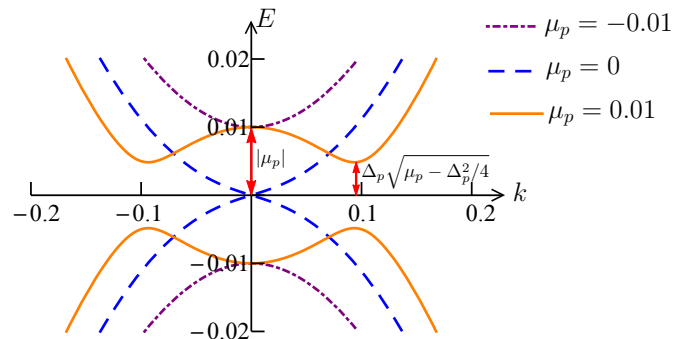


FIG. 1. (Color online) Typical energy spectra of the spinless p SC illustrating the nontopological ($\mu_p = -0.01$), transition ($\mu_p = 0$) and topological regimes ($\mu_p = 0.01$). In all curves we set $\Delta_p = 0.05$.

We consider the scattering of an electron injected from the NM into the p SC with energy E . The incident electron can be normal reflected as an electron, Andreev reflected as a hole, or transmitted into the p SC. The scattering wave function is $\Phi(x) = \Phi_N(x)\Theta(-x) + \Phi_p(x)\Theta(x)$, where $\Theta(x)$ is the Heaviside step function

and

$$\Phi_N(x) = \begin{pmatrix} 1 \\ a \end{pmatrix} e^{ix} + \begin{pmatrix} b \\ 0 \end{pmatrix} e^{-ix}, \quad (2a)$$

$$\Phi_p(x) = c \begin{pmatrix} \gamma_- \\ 1 \end{pmatrix} e^{ik_-x} + d \begin{pmatrix} \gamma_+ \\ 1 \end{pmatrix} e^{ik_+x}, \quad (2b)$$

where a and b are the Andreev and normal reflection amplitudes, respectively, c and d are the transmission coefficients into the p SC, and

$$\gamma_{\pm} = \frac{E + k_{\pm}^2 - \mu_p}{\Delta_p k_{\pm}}. \quad (3)$$

Note that we approximate the wave vector of the electrons and holes in the NM by the Fermi momentum $k_F = \sqrt{2m\mu_N}/\hbar$, valid for $E \ll 1$. The momenta k_{\pm}

of the p SC wave function are solutions of the equation

$$E^2 = (k^2 - \mu_p)^2 + (\Delta_p k)^2. \quad (4)$$

Depending on the energy E of the incoming electron and the chemical potential μ_p , the p SC wave function can either be evanescent with complex solutions of Eq. (4), or involve propagating states corresponding to real solutions of Eq. (4) with positive group velocity. We classify the different solutions in Table I.

The wave functions satisfy the continuity equation $\Phi_p(x)|_{x=0^+} = \Phi_N(x)|_{x=0^-}$ and current conservation condition $J_p \Phi_p(x)|_{x=0^+} - J_N \Phi_N(x)|_{x=0^-} = -2iZ\tau_z \Phi_N(0)$ where the current operators are given by

$$J_N = -2i\partial_x \tau_z, \quad J_p = -2i\partial_x \tau_z + \Delta_p \tau_x. \quad (5)$$

Solving the boundary conditions, we derive the Andreev and normal reflection coefficients

$$a(E) = \frac{\Delta_p(\gamma_+ - \gamma_-) - 2(k_+ - k_-)}{\mathcal{D}_E}, \quad \text{and} \quad (6a)$$

$$b(E) = \frac{(2 - 2iZ - k_+ - k_- - \Omega)(\gamma_- - \gamma_+) + \frac{\Delta_p}{2}(k_+ - k_-)(\gamma_+ \gamma_- + 1)}{\mathcal{D}_E}, \quad (6b)$$

respectively, where

$$\Omega = 1 + (Z - ik_-)(Z - ik_+) - \frac{\Delta_p^2}{4}, \quad \text{and} \quad (7a)$$

$$\mathcal{D}_E = \Omega(\gamma_- - \gamma_+) - \frac{\Delta_p}{2}(k_+ - k_-)(\gamma_+ \gamma_- + 1) - (k_+ - k_-)(\gamma_- + \gamma_+). \quad (7b)$$

μ_p	E	k_-, k_+
$\mu_p \leq \Delta_p^2/4$	$0 \leq E \leq E_2$	k_{I-}, k_{I+}
	$E \geq E_2$	k_{I+}, k_{R+}
$\Delta_p^2/4 \leq \mu_p \leq \Delta_p^2/2$	$0 \leq E \leq E_1$	k_{C-}, k_{C+}
	$E_1 \leq E \leq E_2$	k_{I-}, k_{I+}
	$E \geq E_2$	k_{I+}, k_{R+}
$\mu_p \geq \Delta_p^2/2$	$0 \leq E \leq E_1$	k_{C-}, k_{C+}
	$E_1 \leq E \leq E_2$	k_{R-}, k_{R+}
	$E \geq E_2$	k_{I+}, k_{R+}

TABLE I. Various solutions of Eq. (4) for different values of chemical potential μ_p and energy E , where $E_1 = \Delta_p \sqrt{\mu_p - \Delta_p^2/4}$ and $E_2 = |\mu_p|$. We denote propagating solutions by $k_{R\pm}$, while evanescent solutions are given by $k_{I\pm}$ and $k_{C\pm}$. These are given by $k_{R\pm} = \pm[(\mu_p - \Delta_p^2/2) \pm \sqrt{E^2 - E_1^2}]^{1/2}$, $k_{I\pm} = i[(\Delta_p^2/2 - \mu_p) \pm \sqrt{E^2 - E_1^2}]^{1/2}$ and $k_{C\pm} = \pm[(\mu_p - \Delta_p^2/2) \pm i\sqrt{E_1^2 - E^2}]^{1/2}$.

Within the BTK formalism⁵⁹ the zero-temperature differential conductance is given by

$$G_p(E) = G_0 (1 + |a(E)|^2 - |b(E)|^2), \quad (8)$$

where $G_0 = e^2/h$ is the normal state conductance for a

quantum point contact. Although the general form of $G_p(E)$ is lengthy and unenlightening, relatively simple expressions can be found for the physically interesting case of zero bias, i.e., $E = 0$, which we provide in Table II for the three different regimes of μ_p . In particular, we find that the zero-bias conductance abruptly jumps from $G_p(0) = 0$ in the trivial regime ($\mu_p < 0$) to $G_p(0) = 2$ in the topological regime ($\mu_p > 0$). The quantized conductance is characteristic of the topological state, and can be interpreted as indicating perfect Andreev reflection [i.e., $|a(0)|^2 = 1$, $|b(0)|^2 = 0$] at an interface supporting a Majorana mode^{35,36,38}. It is therefore independent of the barrier strength Z and p -wave pairing potential Δ_p . At the transition point ($\mu_p = 0$) we find $G_p(0) \leq G_0$, with the exact value depending upon Z and Δ_p .

Characteristic plots of the conductance as a function of the energy are shown in Figs. 2 and 3. In general, the tunneling conductance $G_p(E)$ decreases with the barrier strength Z , although in the topological regime the zero-bias conductance is unaffected by Z . Furthermore, it is interesting to note that in the topological regime, the width of the zero-bias peak decreases with Z but

	$\mu_p < 0$	$\mu_p = 0$	$\mu_p > 0$
$a(0)$	0	$-\frac{i\Delta_p}{(Z + \Delta_p/2)^2 + 1 + \Delta_p}$	$-i$
$b(0)$	$-e^{i\varphi}$	$-\frac{(Z + \Delta_p/2)^2 + 1}{(Z + \Delta_p/2)^2 + 1 + \Delta_p} e^{i\varphi}$	0
$\frac{G_p(0)}{G_0}$	0	$1 - \frac{[(Z + \Delta_p/2)^2 + 1]^2 - \Delta_p^2}{[(Z + \Delta_p/2)^2 + 1 + \Delta_p]^2}$	2

TABLE II. Explicit expressions for the zero-bias Andreev reflection coefficient $a(0)$, normal reflection coefficient $b(0)$, and differential conductance $G_p(0)$ for the spinless NM- p SC junction. The results are classified according to the three different regimes of μ_p : the nontopological state ($\mu_p < 0$), the topological phase transition point ($\mu_p = 0$), and the topological state ($\mu_p > 0$). The quantity φ is defined by $\sin \varphi = 2(Z + \sqrt{\Delta_p^2/4 - \mu_p}) / [(Z + \sqrt{\Delta_p^2/4 - \mu_p})^2 + 1]$.

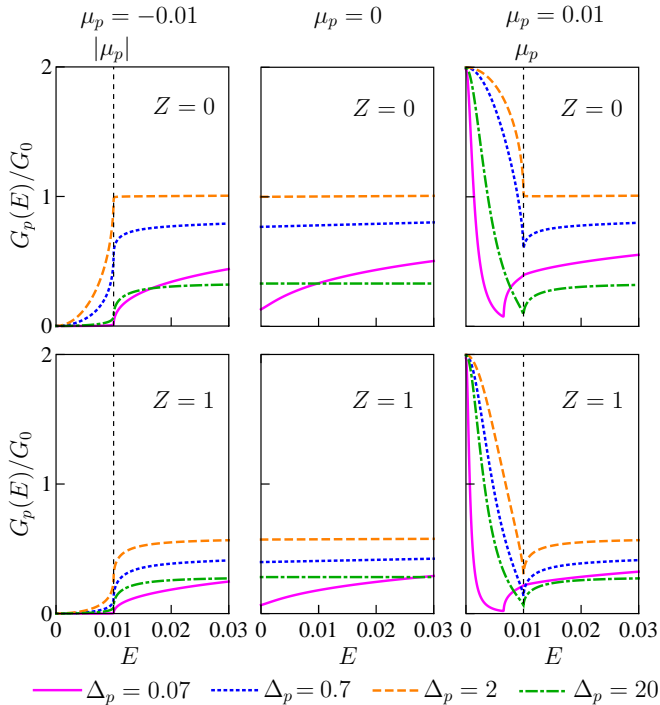


FIG. 2. (Color online) Variation of the tunneling conductance $G_p(E)$ with pairing potential Δ_p and chemical potential μ_p for the spinless NM- p SC junction. The values of the pairing potential Δ_p are given in units of μ_N/k_F , while the chemical potential μ_p and energy E are expressed in units of μ_N . We show typical results for the nontopological ($\mu_p < 0$, left column), transition ($\mu_p = 0$, middle column), and topological ($\mu_p > 0$, right column) regimes, and for barrier strength $Z = 0$ (top row) and $Z = 1$ (bottom row).

shows a nonmonotonic dependence with Δ_p ; the width first increases as Δ_p increases, however, beyond a cer-

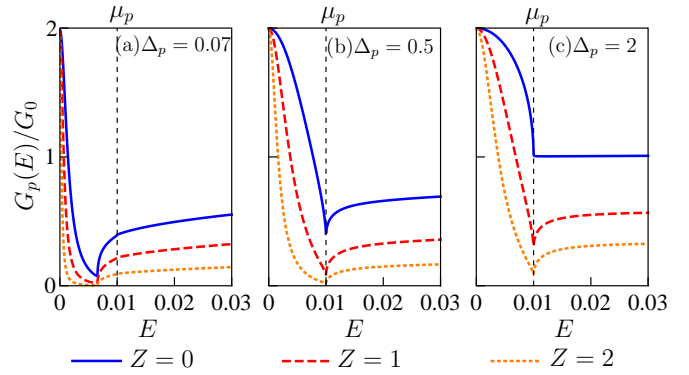


FIG. 3. (Color online) Variation of the tunneling conductance $G_p(E)$ with the barrier strength Z and the pairing potential Δ_p for the spinless NM- p SC junction in the topological regime. The values of the pairing potential Δ_p are given in units of μ_N/k_F while the chemical potential μ_p and energy E are expressed in units of μ_N . Note that the zero-bias conductance is constrained to be $2G_0$ by the topological condition.

tain value of Δ_p , the width decreases with Δ_p . For $\mu_p \leq \Delta_p^2/2$, a singularity appears in the $G_p(E)$ curve at the gap edge $E_2 = |\mu_p|$. On the other hand, as shown in Fig. 3(a), two singularities are visible in the conductance for $\mu_p > \Delta_p^2/2$, corresponding to the edge of the gap at $E_1 = \Delta_p \sqrt{\mu_p - \Delta_p^2/4}$ and the local maximum in the spectrum at $E_2 = \mu_p$.

III. JUNCTION WITH A SPIN-ORBIT-COUPLED NANOWIRE

In its topological phase, the low-energy sector of the spin-orbit-coupled nanowire proposal is formally equivalent to the spinless p -wave superconductor studied above^{6,7,9}. In order to obtain the conductance spectrum and its variation across the topological transition, however, we must examine the full model including spin-orbit coupling and Zeeman splitting. In this section we therefore consider a one-dimensional junction between a spin-split spin-orbit-coupled superconducting wire (SOCSW) and a spinful normal metal (NM), which occupy the regions $x \geq 0$ and $x \leq 0$, respectively. Similar to Sec. II, we model their interface at $x = 0$ by a δ -potential barrier of strength Z . The Hamiltonian in each region is written $H_j(x) = \frac{1}{2} \int dx \bar{\Psi}_j^\dagger(x) \mathcal{H}_j \bar{\Psi}_j(x)$, where $\bar{\Psi}_j(x) = (\psi_{j\uparrow}(x), \psi_{j\downarrow}(x), \psi_{j\downarrow}^\dagger(x), -\psi_{j\uparrow}^\dagger(x))^T$ and $\psi_{j\sigma}^\dagger(x)$ [$\psi_{j\sigma}(x)$] is the creation (annihilation) field operator of an electron with spin σ in region $j = N$ (NM) or S (SOCSW). Using the same unit convention as in the previous section, we write the BdG Hamiltonians of the NM and SOCSW as

$$\mathcal{H}_N = (-\partial_x^2 - 1) \tau_z, \quad (9a)$$

$$\mathcal{H}_S = -\partial_x^2 \tau_x - i\alpha \partial_x \tau_z \sigma_z + V_Z \sigma_x + \Delta_0 \tau_x, \quad (9b)$$

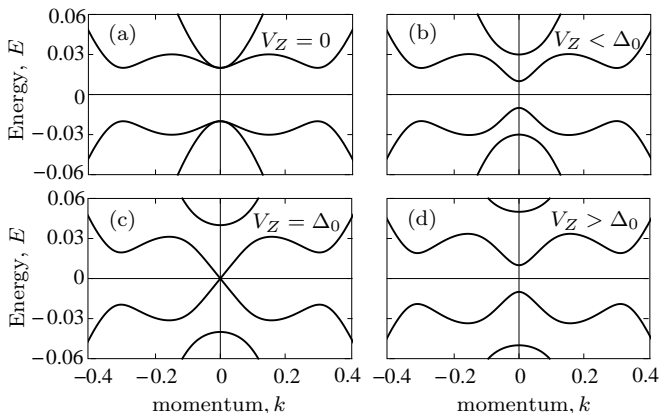


FIG. 4. Energy spectrum of the SOCSW for different values of Zeeman potentials: (a) $V_Z = 0$ (nontopological), (b) $V_Z = 0.01$ (nontopological), (c) $V_Z = 0.02$ (transition), and (d) $V_Z = 0.03$ (topological). In all plots, we set $\alpha = 0.3$ and $\Delta_0 = 0.02$.

where σ_μ (τ_μ) are the Pauli matrices in spin (particle-hole) space, α is the strength of spin-orbit coupling (SOC), V_Z is the Zeeman field, and $\Delta_0 \geq 0$ is the proximity-induced s -wave pairing potential which is assumed to be real. We set the chemical potential of the SOCSW and Zeeman coupling in the lead to be zero, and take uniform electron masses throughout the system.

The positive branches of the BdG spectrum of the SOCSW are given by

$$E_{\pm} = \left(k^4 + \alpha^2 k^2 + \Delta_0^2 + V_Z^2 \pm 2\sqrt{k^4(\alpha^2 k^2 + V_Z^2) + \Delta_0^2 V_Z^2} \right)^{1/2}. \quad (10)$$

As shown in Fig. 4, the energy spectrum is gapped except for $V_Z = \Delta_0$. This value of V_Z marks the topological quantum phase transition between the topologically trivial ($V_Z < \Delta_0$) and nontrivial phases ($V_Z > \Delta_0$)⁴⁻⁷. Although Eq. (10) can be analytically solved for the momenta corresponding to a given energy E , the general expression is unwieldy. In what follows, therefore, we will instead work in the limits of a strong Zeeman field and strong SOC, where more compact results can be obtained.

A. Strong Zeeman splitting

In the limit of strong Zeeman splitting ($V_Z \gg \alpha, \Delta_0$), the quasiparticle excitation spectrum of the SOCSW is split into two spin bands as shown in Fig. 5(a). In the normal state ($\Delta_0 = 0$) the spectrum is approximately given by $\epsilon_{\pm}(k) \approx k^2 \pm V_Z$. The system is then a half-metal, with only one spin-polarized band [$\epsilon_{-}(k)$] occupied. Projecting the full Hamiltonian into this band gives

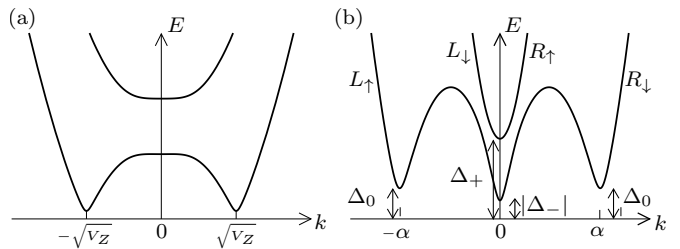


FIG. 5. Energy spectrum of the SOCSW in the limits of (a) strong Zeeman field and (b) strong SOC. For clarity, only the positive energy branches of the spectrum are shown. In panel (b), the spectrum about the minima at $k = 0$ constitute the “interior” branches, while the spectrum about the minima at $k = \pm\alpha$ are the “exterior” branches. Note the different effective gaps for these branches, and the states contributing to the slowly varying left- and right-moving fields, $L_\sigma(x)$ and $R_\sigma(x)$, respectively.

the effective Hamiltonian^{5,6,8}

$$H'_S(k) = \sum_k \left\{ \epsilon_{-}(k) \psi_{S-}^\dagger(k) \psi_{S-}(k) + \left[\tilde{\Delta}_{-}(k) \psi_{S-}^\dagger(k) \psi_{S-}^\dagger(-k) + \text{h.c.} \right] \right\}, \quad (11)$$

where $\tilde{\Delta}_{-}(k) \approx \alpha k \Delta_0 / V_Z$ is a p -wave pairing potential and $\psi_{S-}(\psi_{S-}^\dagger)$ is the annihilation (creation) field operator for $\epsilon_{-}(k)$ band. The projected Hamiltonian is equivalent to the spinless p SC Hamiltonian $H_p(k)$ [Eq. (1)], with the identifications $\mu_p = V_Z$ and $\Delta_p = \alpha \Delta_0 / V_Z$. If the Zeeman field is applied on both sides of the junction such that the NM is also fully spin polarized, then the low-energy sector is identical to the spinless NM- p SC junction studied in Sec. II, and the results obtained above for the differential conductance directly apply.

B. Strong spin-orbit coupling

In the case of strong SOC ($\alpha \gg V_Z, \Delta_0$), the BdG spectrum of the SOCSW has the characteristic form shown in Fig. 5(b). In particular, we note that both the $+$ and $-$ spectra [Eq. (10)] have minima at $k = 0$ (the so-called interior branches), while the $-$ spectrum also has minima at $k = \pm\alpha$ (the exterior branches). For small energies $E \lesssim \Delta_0, V_Z$, we can linearize the Hamiltonian about these minima by introducing the ansatz for the field operators⁶⁴⁻⁶⁶

$$\psi_{S\uparrow}(x) \approx R_\uparrow(x) + L_\uparrow(x) e^{-i\alpha x}, \quad (12a)$$

$$\psi_{S\downarrow}(x) \approx L_\downarrow(x) + R_\downarrow(x) e^{i\alpha x}, \quad (12b)$$

where $R_\sigma(x)$ and $L_\sigma(x)$ represent slowly-varying right- and left-moving fields, respectively; see Fig. 5(b). Inserting this ansatz into the Hamiltonian [Eq. (9b)] and

neglecting all “fast oscillating” terms (involving terms with phase factors $e^{\pm i\alpha x}$), we obtain effective Hamiltonians valid for the states near the interior and exterior branches. Specifically, we write

$$\tilde{H}_S^{(l)} = \frac{1}{2} \int dx \tilde{\Psi}_S^{(l)}(x)^\dagger \tilde{\mathcal{H}}_S^{(l)} \tilde{\Psi}_S^{(l)}(x), \quad (13)$$

where $l = e, i$ denotes the exterior and interior branches, respectively, and the BdG Hamiltonians are written

$$\tilde{\mathcal{H}}_S^{(e)} = -i\alpha\tau_z\sigma_z\partial_x + \Delta_0\tau_x, \quad (14a)$$

$$\tilde{\mathcal{H}}_S^{(i)} = -i\alpha\tau_z\sigma_z\partial_x + V_Z\sigma_x + \Delta_0\tau_x. \quad (14b)$$

The spinors for the interior and exterior branches are defined in terms of the slowly-varying field as $\tilde{\Psi}_S^{(e)}(x) = (L_\uparrow(x), R_\downarrow(x), R_\downarrow^\dagger(x), -L_\uparrow^\dagger(x))^\top$ and $\tilde{\Psi}_S^{(i)}(x) = (R_\uparrow(x), L_\downarrow(x), L_\downarrow^\dagger(x), -R_\uparrow^\dagger(x))^\top$.

We consider an electron with energy E and spin σ injected into the SOCSW from the NM. The wave function in the NM is given by

$$\Phi_{N\sigma}(x) = \begin{pmatrix} \delta_{\sigma\uparrow} \\ \delta_{\sigma\downarrow} \\ 0 \\ 0 \end{pmatrix} e^{ix} + \begin{pmatrix} b_{\sigma\uparrow} \\ b_{\sigma\downarrow} \\ 0 \\ 0 \end{pmatrix} e^{-ix} + \begin{pmatrix} 0 \\ 0 \\ a_{\sigma\downarrow} \\ a_{\sigma\uparrow} \end{pmatrix} e^{ix}, \quad (15)$$

where $\delta_{\sigma\sigma'}$ is the Kronecker symbol. The coefficients $a_{\sigma\sigma'}$ and $b_{\sigma\sigma'}$ are the amplitudes for Andreev and normal reflection, respectively. Note that due to the SOC in the SOCSW, both spin-flip and spin-preserving reflection processes are allowed. The wave function in the SOCSW is a superposition of solutions on the exterior and interior branches

$$\begin{aligned} \Phi_{S\sigma}(x) = & \\ & c_{\sigma 1}^{(i)} \begin{pmatrix} -u_- \\ \text{sgn}(\Delta_-)v_- \\ -\text{sgn}(\Delta_-)v_- \\ u_- \end{pmatrix} e^{ik_-^{(i)}x} + c_{\sigma 2}^{(i)} \begin{pmatrix} u_+ \\ v_+ \\ v_+ \\ u_+ \end{pmatrix} e^{ik_+^{(i)}x} \\ & + c_{\sigma 1}^{(e)} \begin{pmatrix} v_0 \\ 0 \\ u_0 \\ 0 \end{pmatrix} e^{i(k_0^{(e)} - \alpha)x} + c_{\sigma 2}^{(e)} \begin{pmatrix} 0 \\ u_0 \\ 0 \\ v_0 \end{pmatrix} e^{i(k_0^{(e)} + \alpha)x}, \quad (16) \end{aligned}$$

where the first line on the right-hand side gives contributions from the interior branches, while the second line originates from the exterior branches. Note that the coefficients $c_{\sigma(1,2)}^{(i)}$ and $c_{\sigma(1,2)}^{(e)}$ are the transmission coefficients into the SOCSW. The elements of the wave function are given by

$$u_\nu^2 = \begin{cases} (E + \sqrt{E^2 - \Delta_\nu^2})/2E, & \text{for } E \geq |\Delta_\nu|, \\ (E + i\sqrt{\Delta_\nu^2 - E^2})/2|\Delta_\nu|, & \text{for } 0 \leq E < |\Delta_\nu|, \end{cases} \quad (17)$$

and

$$v_\nu^2 + u_\nu^2 = \begin{cases} 1, & \text{for } E \geq |\Delta_\nu|, \\ E/|\Delta_\nu|, & \text{for } 0 \leq E < |\Delta_\nu|, \end{cases} \quad (18)$$

where $\nu = \pm, 0$, and $\Delta_\pm = \Delta_0 \pm V_Z$. The wave vectors appearing in Eq. (16) are $k_\pm^{(i)} = \sqrt{E^2 - \Delta_\pm^2}/\alpha$ for the interior branches, and $k_0^{(e)} = \sqrt{E^2 - \Delta_0^2}/\alpha$ for the exterior branches.

The wave functions satisfy the continuity and current conservation boundary conditions

$$\Phi_{S\sigma}(x)|_{x=0^+} = \Phi_{N\sigma}(x)|_{x=0^-}, \quad (19a)$$

$$J_S \Phi_{S\sigma}(x)|_{x=0^+} - J_N \Phi_{N\sigma}(x)|_{x=0^-} = -2iZ\tau_z \Phi_{N\sigma}(0), \quad (19b)$$

where the current operators are given by

$$J_N = -2i\partial_x\tau_z, \quad J_S = -2i\partial_x\tau_z + \alpha\tau_z\sigma_z. \quad (20)$$

In the limit of strong SOC ($\alpha \gg V_Z, \Delta_0$), we ignore terms proportional to $k_-^{(i)}$, $k_+^{(i)}$, $k_0^{(e)} \ll 1$ in the current conservation equation. Expressions for the Andreev and normal reflection coefficients found from solving these equations are given in Appendix A.

The zero-temperature differential tunneling conductance $G_S(E)$ is obtained from the BTK formula

$$G_S(E) = G_0 \left(2 + \sum_{\sigma, \xi=\uparrow, \downarrow} \{|a_{\sigma\xi}(E)|^2 - |b_{\sigma\xi}(E)|^2\} \right). \quad (21)$$

Although the general expression is complicated, compact forms for the reflection coefficients and the conductance at zero bias are presented in Table III. As in the spinless NM- p SC junction studied above, the zero-bias conductance $G_S(0)$ is discontinuous across the topological phase transition. In the topological regime ($V_Z > \Delta_0$) the zero-bias conductance takes the quantized value $G_S(0) = 2$. This implies that the Andreev reflection coefficients in Eq. (21) exactly cancel the normal reflection coefficients; moreover, from Table III it can be verified that $\sum_{\sigma, \xi} |a_{\sigma\xi}(0)|^2 = \sum_{\sigma, \xi} |b_{\sigma\xi}(0)|^2 = 1$. This can be understood in terms of the existence of a single Majorana mode at the interface which couples to one of the two channels in the normal region^{35,38}. While there is perfect Andreev reflection in this channel, in the other channel we have perfect normal reflection. In the nontopological regime, on the other hand, $G_S(0)$ takes on nonuniversal values and is dependent upon Z and α . In particular, the zero-bias conductance in the nontopological phase can strongly exceed the quantized value in the topological state: for the gapped nontopological state ($V_Z < \Delta_0$) and at the topological transition point ($V_Z = \Delta_0$), we find the maximum values $G_S(0) = 4$ and $G_S(0) = 3$, respectively, which are realized for $Z = 0$ and $\alpha = 2$.

We plot the calculated conductance as a function of energy in Figs. 6 and 7. In the former we show examples

	$V_Z < \Delta_0$	$V_Z = \Delta_0$	$V_Z > \Delta_0$
$a_{\uparrow\uparrow}(0)$	0	$\frac{\alpha[1 + (Z + i\alpha/2)^2]}{D_1 D_2}$	$\frac{1 + (Z + i\alpha/2)^2}{D_1}$
$a_{\uparrow\downarrow}(0)$	$-\frac{2i\alpha}{D_1}$	$-\frac{i\alpha}{D_1}$	$\frac{i}{2} - \frac{i\alpha}{D_1}$
$a_{\downarrow\uparrow}(0)$	$-\frac{2i\alpha}{D_1}$	$-i\alpha \left(\frac{1}{D_1} + \frac{1}{D_2} \right)$	$-\frac{i}{2} - \frac{i\alpha}{D_1}$
$a_{\downarrow\downarrow}(0)$	0	$\frac{\alpha[1 + (Z - i\alpha/2)^2]}{D_1 D_2}$	$\frac{1 + (Z - i\alpha/2)^2}{D_1}$
$b_{\uparrow\uparrow}(0)$	$\frac{2[(i + Z)^2 + (\alpha/2)^2]}{D_1}$	$\frac{2[(i + Z)^2 + (\alpha/2)^2][D_2 - \alpha/2]}{D_1 D_2}$	$\frac{(i + Z)^2 + (\alpha/2)^2}{D_1}$
$b_{\uparrow\downarrow}(0)$	0	$\frac{-i\alpha(1 - iZ + \alpha/2)^2}{D_1 D_2}$	$\frac{-i(1 - iZ + \alpha/2)^2}{D_1}$
$b_{\downarrow\uparrow}(0)$	0	$\frac{i\alpha(-1 + iZ + \alpha/2)^2}{D_1 D_2}$	$\frac{i(-1 + iZ + \alpha/2)^2}{D_1}$
$b_{\downarrow\downarrow}(0)$	$\frac{2[(i + Z)^2 + (\alpha/2)^2]}{D_1}$	$\frac{2[(i + Z)^2 + (\alpha/2)^2][D_2 - \alpha/2]}{D_1 D_2}$	$\frac{(i + Z)^2 + (\alpha/2)^2}{D_1}$
$\frac{G_S(0)}{G_0}$	$\frac{16\alpha^2}{D_1^2}$	$2\alpha \left(\frac{4}{D_1} - \frac{1}{D_2} \right)$	2

TABLE III. Zero-bias values of the Andreev reflection coefficients $a_{\sigma\sigma'}(0)$, normal reflection coefficients $b_{\sigma\sigma'}(0)$, and differential conductance $G_S(0)$ in the strong SOC limit of the NM-SOCSW junction. The three columns give the values in the nontopological ($V_Z < \Delta_0$), transition ($V_Z = \Delta_0$) and topological ($V_Z > \Delta_0$) regimes. The terms $D_{1,2}$ are given by $D_1 = 2[1 + Z^2 + (\alpha/2)^2]$ and $D_2 = Z^2 + (1 + \alpha/2)^2$.

of the conductance spectra in the nontopological, transition, and topological regimes, while the latter explores more fully the variation of the conductance spectra in the topological state away from zero bias. The conductance spectra show a much more complicated structure than those in the spinless NM- p SC junction, reflecting the presence of three distinct gaps (Δ_+ , $|\Delta_-|$, Δ_0) in the strong SOC limit of the SOCSW. Indeed, at the energy corresponding to each gap we observe a nonanalyticity in the conductance spectrum. Although there is considerable variation in the conductance spectrum as a function of energy, a number of trends can be discerned: increasing Z tends to suppress the conductance, the energy variation of the conductance is nonmonotonic in general with cusplike structures at specific energies, and the energy variation of the conductance is stronger near zero energy for larger values of Z . While the conductance at first tends to be enhanced by increasing the SOC, the conductance eventually goes through a maximum before monotonically decreasing. Similarly, the SOC increases the width of the zero-bias peak in the topological regime, but beyond a certain SOC strength it decreases again. The basic finding is that, other than the universal quantized Majorana peak at zero energy, the tunneling conductance shows interesting and nontrivial dependence on Z and E in the topological phase. In particular, an interesting conclusion of our theory is that the zero-bias

conductance could be quantized in the topological phase for small values of Z without developing a peak in the tunneling conductance at all.

Note that the above discussion holds true also for the case where the Zeeman coupling in the lead or the chemical potential μ_S of the SOCSW are nonzero. For the case where $|\Delta_-| < \Delta_0$, the zero-bias peak formed in the topological regime is within an energy range of $|\Delta_-|$. Since the topological gap $|\Delta_-| = |\sqrt{\Delta_0^2 + \mu_S^2} - V_Z|$ decreases with the absolute value of the chemical potential $|\mu_S|$, the width of the zero-bias peak decreases with $|\mu_S|$.

IV. SUMMARY

Using the BTK formalism we have analytically studied the zero-temperature tunneling conductance spectra of NS junctions involving topological superconductors. Finite temperature effects within this formalism simply lead to thermal broadening of the zero-temperature conductance and can be included in the theory numerically by introducing an integration over the Fermi function⁶⁷. As in the BTK paper⁵⁹, the finite-voltage conductances are found to depend on the strength of the barrier at the interface, which is parameterized by the dimensionless parameter Z . Specifically, we have examined a spinless NM- p SC junction and a spinful NM-SOCSW junction,

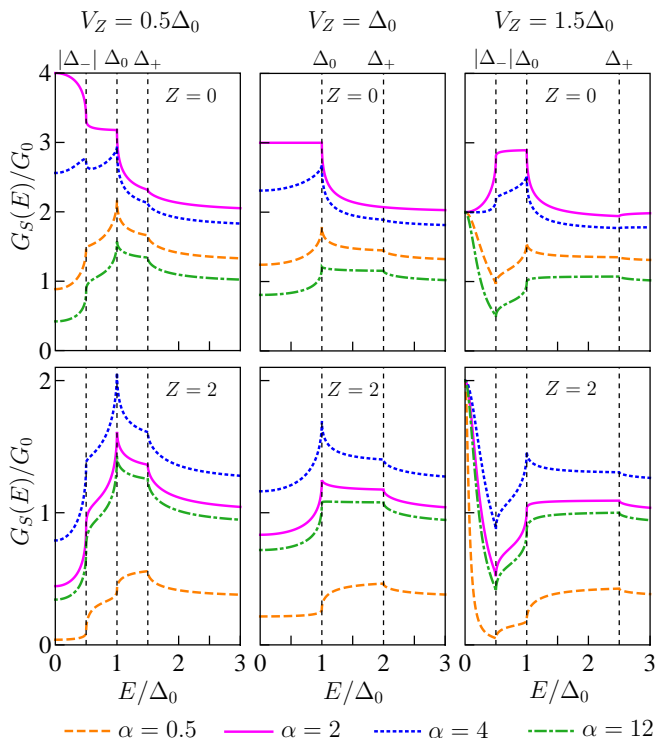


FIG. 6. (Color online) Variation of the tunneling conductance $G_S(E)$ with SOC strength α and Zeeman field V_Z in the strong SOC limit of the NM-SOCSW junction. We present typical results for the nontopological ($V_Z < \Delta_0$, left column), transition ($V_Z = 0$, middle column), and topological ($V_Z > \Delta_0$, right column) regimes, and for barrier strength $Z = 0$ (top row) and $Z = 2$ (bottom row). In all plots we set $\Delta_0 = 0.001$. The values of Δ_0 and V_Z are given in units of μ_N , while the values of α are expressed in units of μ_N/k_F .

paying particular attention to the change in the zero-bias conductance across the topological phase transition. We explicitly demonstrate that the zero-temperature zero-bias conductance is quantized at a value of $2e^2/h$ in the topological regime, in agreement with effective models of these systems based on a single Majorana mode coupled to a normal channel. Despite this quantization at zero voltage, the zero-bias conductance only develops a peak (or a local maximum) as a function of voltage for barriers with sufficiently large Z parameter, or for small and large SOC strength. These parameters also control the width of this peak. In the nontopological regime, on the other hand, the conductance takes nonuniversal values depending upon the details of the system. In both cases the conductance spectrum away from zero bias shows considerable variation with the details of the junction. Our calculated BTK conductance also shows that the conductance is finite inside the superconducting gap region because of the finite barrier transparency, providing a possible mechanism for the observed “soft gap” feature in the experimental studies^{9,11–14}. This effect is qualitatively similar to the “inverse proximity effect” at the NS

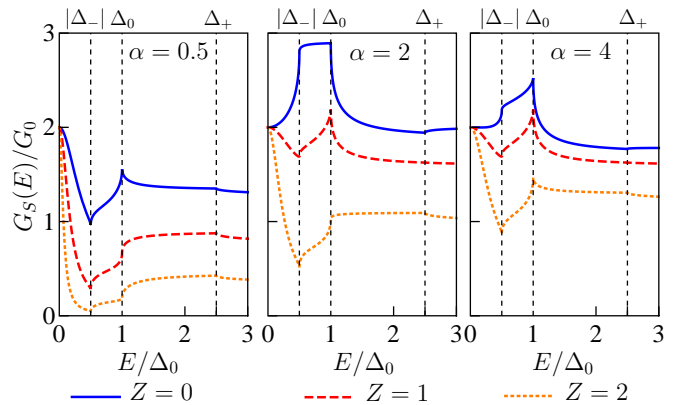


FIG. 7. (Color online) Variation of the tunneling conductance $G_S(E)$ with interface barrier strength Z and spin-orbit coupling strength α for the strong SOC limit of the NM-SOCSW junction in the topological regime. We set $\Delta_0 = 0.001$ and $V_Z = 1.5\Delta_0$. The values of Δ_0 and V_Z are given in units of μ_N , while the values of α are expressed in units of μ_N/k_F . Note that in all cases the zero-bias conductance is equal to $2G_0$, consistent with the topological state.

interface arising from the finite barrier at the interface as discussed in the recent literature⁵⁰, although other possible physical mechanisms for the soft gap behavior have also been proposed⁶⁸. We mention finally that our theory is for a single NS junction which effectively assumes the existence of only a single Majorana mode at the NS interface (with the other Majorana being located infinitely far away) and thus Majorana splitting^{45,69–71} due to the wave function overlap between two Majorana modes is not germane to our theory (but can be included if necessary in a future generalization).

Finally, we emphasize that one of the most salient features of our theoretical work is that it is completely analytical within a continuum model in contrast to most theoretical works on Majorana nanowires which focus on numerical simulations within a tight-binding lattice model. All the microscopic details of the complex normal-superconductor tunneling process are simply subsumed in a single phenomenological parameter Z (“the interface barrier strength” of the BTK formalism) allowing our theory a great deal of flexibility for actual modeling of the Majorana nanowire experimental results, since the realistic microscopic details of the NS interface are rarely known in the actual experimental nanowire setups. It is gratifying that our analytical model captures the essential features of the Majorana nanowire experiments through our finding of the Majorana zero-bias conductance quantization and soft gap feature, with the interesting prediction that for strong metallic junction (i.e., for very low interface barrier or a small value of Z) the Majorana zero-bias conductance may not necessarily be a peak in the tunneling conductance although it would still be quantized since the Majorana zero mode necessarily implies perfect Andreev reflection.

V. ACKNOWLEDGMENTS

We thank H.-Y. Hui, X. Liu, and D. Rainis for fruitful discussions. This work was supported by Microsoft Station Q, LPS-CMTC, and JQI-NSF-PFC.

Appendix A: Andreev and normal reflection coefficients for the NM-SOCSW junction

Solving the boundary equations, we obtain the Andreev (normal) reflection coefficients $a_{\sigma\sigma'}$ ($b_{\sigma\sigma'}$) as

$$a_{\uparrow\uparrow}(E) = -\frac{\alpha u_0 v_0 [u_- v_+ - \text{sgn}(\Delta_-) u_+ v_-] [1 + (Z + i\frac{\alpha}{2})^2]}{\mathcal{D}_E^{(1)} \mathcal{D}_E^{(2)}}, \quad (\text{A1})$$

$$a_{\uparrow\downarrow}(E) = \alpha u_0 \left[\frac{v_+}{\mathcal{D}_E^{(1)}} + \text{sgn}(\Delta_-) \frac{v_-}{\mathcal{D}_E^{(2)}} \right], \quad (\text{A2})$$

$$a_{\downarrow\uparrow}(E) = \alpha v_0 \left(\frac{u_+}{\mathcal{D}_E^{(1)}} + \frac{u_-}{\mathcal{D}_E^{(2)}} \right), \quad (\text{A3})$$

$$a_{\downarrow\downarrow}(E) = -\frac{\alpha u_0 v_0 [u_- v_+ - \text{sgn}(\Delta_-) u_+ v_-] [1 + (Z - i\frac{\alpha}{2})^2]}{\mathcal{D}_E^{(1)} \mathcal{D}_E^{(2)}}, \quad (\text{A4})$$

$$b_{\uparrow\uparrow}(E) = b_{\downarrow\downarrow}(E) \quad (\text{A5})$$

$$= - \left[(i + Z)^2 + \left(\frac{\alpha}{2} \right)^2 \right] \times \left\{ \frac{\text{sgn}(\Delta_-) v_0^2 v_- v_+ [Z^2 + (\frac{\alpha}{2} - 1)^2] - u_0 v_0 [u_- v_+ + \text{sgn}(\Delta_-) u_+ v_-] [1 + Z^2 + (\frac{\alpha}{2})^2] + u_0^2 u_- u_+ [Z^2 + (1 + \frac{\alpha}{2})^2]}{\mathcal{D}_E^{(1)} \mathcal{D}_E^{(2)}} \right\},$$

$$b_{\uparrow\downarrow}(E) = \frac{\alpha u_0^2 [u_- v_+ - \text{sgn}(\Delta_-) u_+ v_-] (1 - iZ + \frac{\alpha}{2})^2}{\mathcal{D}_E^{(1)} \mathcal{D}_E^{(2)}}, \quad (\text{A6})$$

$$b_{\downarrow\uparrow}(E) = \frac{\alpha v_0^2 [u_- v_+ - \text{sgn}(\Delta_-) u_+ v_-] (-1 + iZ + \frac{\alpha}{2})^2}{\mathcal{D}_E^{(1)} \mathcal{D}_E^{(2)}}, \quad (\text{A7})$$

where $\mathcal{D}_E^{(1)} = u_0 u_+ [Z^2 + (\alpha/2 + 1)^2] - v_0 v_+ [Z^2 + (\alpha/2 - 1)^2]$ and $\mathcal{D}_E^{(2)} = u_0 u_- [Z^2 + (\alpha/2 + 1)^2] - \text{sgn}(\Delta_-) v_0 v_- [Z^2 + (\alpha/2 - 1)^2]$.

¹ N. Read and D. Green, Phys. Rev. B **61**, 10267 (2000).

² A. Kitaev, Phys. Usp. **44**, 131 (2001).

³ C. Nayak, S. H. Simon, A. Stern, M. Freedman, and S. Das Sarma, Rev. Mod. Phys. **80**, 1083 (2008).

⁴ Jay D. Sau, R. M. Lutchyn, S. Tewari, and S. Das Sarma, Phys. Rev. Lett. **104**, 040502 (2010).

⁵ Jay D. Sau, S. Tewari, R. M. Lutchyn, T. D. Stanescu and S. Das Sarma, Phys. Rev. B **82**, 214509 (2010).

⁶ R. M. Lutchyn, Jay D. Sau, and S. Das Sarma, Phys. Rev. Lett. **105**, 077001 (2010).

⁷ Y. Oreg, G. Refael, and F. von Oppen, Phys. Rev. Lett. **105**, 177002 (2010).

⁸ J. Alicea, Phys. Rev. B **81**, 125318 (2010).

⁹ V. Mourik, K. Zuo, S. M. Frolov, S. R. Plissard, E. P. A. M. Bakkers, and L. P. Kouwenhoven, Science **336**, 1003

(2012).

¹⁰ L. P. Rokhinson, X. Liu, and J. K. Furdyna, Nat. Phys. **8**, 795 (2012).

¹¹ M. T. Deng, C. L. Yu, G. Y. Huang, M. Larrson, P. Caroff, and H. Q. Xu, Nano Lett. **12**, 6414 (2012).

¹² A. Das, Y. Ronen, Y. Most, Y. Oreg, M. Heiblum, and H. Shtrikman, Nat. Phys. **8**, 887 (2012).

¹³ A. D. K. Finck, D. J. Van Harlingen, P. K. Mohseni, K. Jung, and X. Li, Phys. Rev. Lett. **110**, 126406 (2013).

¹⁴ H. O. H. Churchill, V. Fatemi, K. Grove-Rasmussen, M. T. Deng, P. Caroff, H. Q. Xu, and C. M. Marcus, Phys. Rev. B **87**, 241401(R) (2013).

¹⁵ E. J. H. Lee, X. Jiang, M. Houzet, R. Aguado, C. M. Lieber, and S. De Franceschi, Nat. Nanotechnol. **9**, 79 (2014).

- ¹⁶ L. Fu and C. L. Kane, Phys. Rev. Lett. **100**, 096407 (2008).
- ¹⁷ L. Fu and C. L. Kane, Phys. Rev. B **79**, 161408(R) (2009).
- ¹⁸ T.-P. Choy, J. M. Edge, A. R. Akhmerov, and C. W. J. Beenakker, Phys. Rev. B **84**, 195442 (2011).
- ¹⁹ S. Mi, D. I. Pikulin, M. Wimmer, and C. W. J. Beenakker Phys. Rev. B **87**, 241405(R) (2013).
- ²⁰ C. Zhang, S. Tewari, R. M. Lutchyn, and S. Das Sarma, Phys. Rev. Lett. **101**, 160401 (2008).
- ²¹ M. Sato, Y. Takahashi, and S. Fujimoto, Phys. Rev. Lett. **103**, 020401 (2009).
- ²² M. Duckheim and P. W. Brouwer, Phys. Rev. B **83**, 054513 (2011).
- ²³ S. B. Chung, H.-J. Zhang, X.-L. Qi and S.-C. Zhang, Phys. Rev. B **84**, 060510(R) (2011).
- ²⁴ S. Takei and V. Galitski, Phys. Rev. B **86**, 054521 (2012).
- ²⁵ L. Mao, M. Gong, E. Dumitrescu, S. Tewari, and C. Zhang, Phys. Rev. Lett. **108**, 177001 (2012).
- ²⁶ Jay D. Sau and S. Das Sarma, Nat. Commun. **3**, 964 (2012).
- ²⁷ Y. Kim, M. Cheng, B. Bauer, R. M. Lutchyn, and S. Das Sarma, Phys. Rev. B **90**, 060401(R) (2014).
- ²⁸ P. M. R. Brydon, S. Das Sarma, H.-Y. Hui, and Jay D. Sau, Phys. Rev. B **91**, 064505 (2015).
- ²⁹ H.-Y. Hui, P. M. R. Brydon, Jay D. Sau and S. Das Sarma, Sci. Rep. **5**, 8880 (2015).
- ³⁰ J. Alicea, Rep. Prog. Phys. **75**, 076501 (2012).
- ³¹ S. Das Sarma, M. Freedman, and C. Nayak, arXiv:1501.02813.
- ³² T. D. Stanescu and S. Tewari, J. Phys. Condens. Matter **25**, 233201 (2013).
- ³³ S. R. Elliott and M. Franz, Rev. Mod. Phys. **87**, 137 (2015).
- ³⁴ K. Sengupta, I. Žutić, H.-J. Kwon, V. M. Yakovenko, and S. Das Sarma, Phys. Rev. B **63**, 144531 (2001).
- ³⁵ K. T. Law, P. A. Lee, and T. K. Ng, Phys. Rev. Lett. **103**, 237001 (2009).
- ³⁶ K. Flensberg, Phys. Rev. B **82**, 180516 (2010).
- ³⁷ M. Wimmer, A. R. Akhmerov, J. P. Dahlhaus, and C. W. J. Beenakker, New. J. Phys. **13**, 053016 (2011).
- ³⁸ X. Liu, Jay D. Sau, and S. Das Sarma, arxiv:1501.07273.
- ³⁹ C.-H. Lin, Jay D. Sau and S. Das Sarma, Phys. Rev. B **86**, 224511 (2012).
- ⁴⁰ F. Pientka, G. Kells, A. Romito, P. W. Brouwer, and F. von Oppen, Phys. Rev. Lett. **109**, 227006 (2012).
- ⁴¹ G. Kells, D. Meidan, and P. W. Brouwer, Phys. Rev. B **86**, 100503(R) (2012).
- ⁴² J. Liu, A. C. Potter, K. T. Law, and P. A. Lee, Phys. Rev. Lett. **109**, 267002 (2012).
- ⁴³ D. Bagrets and A. Altland, Phys. Rev. Lett. **109**, 227005 (2012).
- ⁴⁴ D. I. Pikulin, J. P. Dahlhaus, M. Wimmer, H. Schomerus, and C. W. J. Beenakker, New. J. Phys. **14**, 125011 (2012).
- ⁴⁵ D. Rainis, L. Trifunovic, J. Klinovaja, and D. Loss, Phys. Rev. B **87**, 024515 (2013).
- ⁴⁶ D. Roy, N. Bondyopadhyaya, and S. Tewari, Phys. Rev. B **88**, 020502(R) (2013).
- ⁴⁷ C. Qu, Y. Zhang, L. Mao, and C. Zhang, arXiv:1109.4108 (unpublished).
- ⁴⁸ T. D. Stanescu, R. M. Lutchyn, and S. Das Sarma, Phys. Rev. B **84**, 144522 (2011).
- ⁴⁹ E. Prada, P. San-Jose, and R. Aguado, Phys. Rev. B **86**, 180503(R) (2012).
- ⁵⁰ T. D. Stanescu, R. M. Lutchyn, and S. Das Sarma, Phys. Rev. B **90**, 085302 (2014).
- ⁵¹ D. Roy, C. J. Bolech, and N. Shah, Phys. Rev. B **86**, 094503 (2012).
- ⁵² D. Roy, C. J. Bolech, and N. Shah, arxiv:1303.7036.
- ⁵³ J. J. He, T. K. Ng, P. A. Lee, and K. T. Law, Phys. Rev. Lett. **112**, 037001 (2014).
- ⁵⁴ Z. Yan and S. Wan, New J. Phys. **16** 093004 (2014).
- ⁵⁵ S. Rex and A. Sudbø, Phys. Rev. B **90**, 115429 (2014).
- ⁵⁶ M. Thakurathi, O. Deb and D. Sen, arxiv:1412.0072.
- ⁵⁷ Z. Yan and S. Wan, arxiv:1411.5919v2.
- ⁵⁸ K. Sun and N. Shah, Phys. Rev. B **91**, 144508 (2015).
- ⁵⁹ G. E. Blonder, M. Tinkham and T. M. Klapwijk, Phys. Rev. B **25**, 4515 (1982).
- ⁶⁰ Y. Tanaka and S. Kashiwaya, Phys. Rev. Lett. **74**, 3451 (1995).
- ⁶¹ S. Kashiwaya and Y. Tanaka, Rep. Prog. Phys. **63**, 1641 (2000).
- ⁶² Y. Tanaka, Y. Mizuno, T. Yokoyama, K. Yada, and M. Sato, Phys. Rev. Lett. **105**, 097002 (2010).
- ⁶³ S. Takami, K. Yada, A. Yamaka, M. Sato, and Y. Tanaka, J. Phys. Soc. Jpn. **83**, 064705 (2014).
- ⁶⁴ B. Braunecker, G. I. Japaridze, J. Klinovaja, and D. Loss, Phys. Rev. B **82**, 045127 (2010).
- ⁶⁵ J. Klinovaja and D. Loss, Phys. Rev. B **86**, 085408 (2012).
- ⁶⁶ J. Klinovaja, P. Stano, and D. Loss, Phys. Rev. Lett. **109**, 236801 (2012).
- ⁶⁷ E. Dumitrescu, B. Roberts, S. Tewari, Jay D. Sau, and S. Das Sarma, Phys. Rev. B **91**, 094505 (2015).
- ⁶⁸ S. Takei, B. M. Fregoso, H.-Y. Hui, A. M. Lobos, and S. Das Sarma, Phys. Rev. Lett. **110**, 186803 (2013).
- ⁶⁹ M. Cheng, R. M. Lutchyn, V. Galitski, and S. Das Sarma, Phys. Rev. Lett. **103**, 107001 (2009).
- ⁷⁰ M. Cheng, R. M. Lutchyn, V. Galitski, and S. Das Sarma, Phys. Rev. B **82**, 094504 (2010).
- ⁷¹ S. Das Sarma, Jay D. Sau and T. D. Stanescu, Phys. Rev. B **86** 220506(R) (2012).